THE JOURNAL OF BIOLOGICAL CHEMISTRY VOL. 287, NO. 50, pp. 41569–41575, December 7, 2012
Published in the U.S.A.

Crystal Structures of Tubulin Acetyltransferase Reveal a Conserved Catalytic Core and the Plasticity of the Essential N Terminus*[S]

Received for publication, September 20, 2012, and in revised form, October 26, 2012
Published, JBC Papers in Press, October 26, 2012, DOI 10.1074/jbc.C112.421222

Vasilisa Kormendi[‡], Agnieszka Szyk[‡], Grzegorz Piszczek[§], and Antonina Roll-Mecak[‡§1]

From the [‡]Cell Biology and Biophysics Unit, NINDS, and the [§]NHLBI, National Institutes of Health, Bethesda, Maryland 20892

Background: Tubulin acetyltransferase acetylates α-tubulin in the microtubule lumen.
Results: We present the first crystal structure of TAT and analyze substrate binding molecular determinants. The structure of an inactive mutant reveals a stable domain-swapped dimer.
Conclusion: TAT consists of a conserved core and structurally plastic N terminus essential for activity.
Significance: Our structure provides a rational platform for mechanistic dissection of tubulin acetylation.

Tubulin acetyltransferase (TAT) acetylates Lys-40 of α-tubulin in the microtubule lumen. TAT is inefficient, and its activity is enhanced when tubulin is incorporated in microtubules. Acetylation is associated with stable microtubules and regulates the binding of microtubule motors and associated proteins. TAT is important in neuronal polarity and mechanosensation, and decreased tubulin acetylation levels are associated with axonal transport defects and neurodegeneration. We present the first structure of TAT in complex with acetyl-CoA (Ac-CoA) at 2.7 Å resolution. The structure reveals a conserved stable catalytic core shared with other GCN5 superfamily acetyltransferases consisting of a central β-sheet flanked by α-helices and a C-terminal β-hairpin unique to TAT. Structure-guided mutagenesis establishes the molecular determinants for Ac-CoA and tubulin substrate recognition. The wild-type TAT construct is a monomer in solution. We identify a metastable interface between the conserved core and N-terminal domain that modulates the oligomerization of TAT in solution and is essential for activity. The 2.45 Å resolution structure of an inactive TAT construct with an active site point mutation near this interface reveals a domain-swapped dimer in which the functionally essential N terminus shows evidence of marked structural plasticity. The sequence segment corresponding to this structurally plastic region in TAT has been implicated in substrate recognition in other GCN5 superfamily acetyltransferases. Our structures provide a rational platform for the mechanistic dissection of TAT activity and the design of TAT inhibitors with therapeutic potential in neuronal regeneration.

Microtubules are dynamic polymers essential for cell motility, cell division, and intracellular transport. They are subject to multiple levels of regulation by cellular effectors and diverse posttranslational modifications, including acetylation, detyrosination/tyrosination, polyglutamylation, and polyglycylation. These chemical modifications are thought to locally adapt microtubules for specific functions by directly modifying their dynamics or through differential recruitment of motors, microtubule-associated proteins, or signaling molecules (1, 2).

Tubulin acetyltransferase (TAT)[2] acetylates Lys-40 of α-tubulin in most eukaryotes. TAT shows preference for tubulin already incorporated in microtubules (3, 4), and acetylation is associated predominantly with stable microtubules such as those found in cilia (5, 6) and axons (7). Acetylation regulates the interaction between microtubules and motors as well as membranous organelles (1). For example, kinesin 1 is recruited preferentially to neurites enriched in acetylation, and tubulin hyperacetylation via pharmacological inhibition of the tubulin deacetylase HDAC6 disrupts polarized trafficking, leading to mislocalization of neurite-specific cargoes (8). Consistent with these *in vivo* findings, kinesin 1 preferentially binds acetylated microtubules *in vitro* and has reduced speed on nonacetylated axonemes (8). Tubulin acetylation has been also implicated in regulating the activity of the Na^+/K^+ pump (9), and recent studies show that the endoplasmic reticulum associates and slides primarily along acetylated microtubules (10). A decrease in tubulin acetylation levels has been associated with axonal transport defects as well as neurodegenerative disorders, including Huntington, ALS, and Alzheimer (1).

Tubulin was the first acetylated cytoplasmic protein to be isolated (11, 12); however, the identity of the tubulin acetyltransferase was discovered only recently as MEC-17, a gene required for the function of touch receptor neurons in *Caenorhabditis elegans* (3, 4). TAT belongs to the superfamily of GCN5-related *N*-acetyltransferases (GNAT (13)) and shows high sequence conservation from flagellates to humans (3, 4) (supplemental Fig. 1), with more than 96% identity among mammalian orthologs. TAT has the four sequence motifs characteristic of the GNAT superfamily (Motifs C, D, A, and B (13, 14)). Motif A shows the strongest conservation; Motif C the most divergence throughout the TAT family and the GNAT superfamily (13).

* This work was supported, in whole or in part, by the intramural program of the National Institutes of Health (to A. R. M.).
[S] This article contains supplemental Fig. 1.
The atomic coordinates and structure factors (codes 4H6Z and 4H6U) have been deposited in the Protein Data Bank (http://wwpdb.org/).
[1] A Searle Scholar. To whom correspondence should be addressed: Cell Biology and Biophysics Unit, Porter Neuroscience Research Center, National Institutes of Health, Bldg. 35, Rm. 3B-203, 35 Convent Dr., MSC 3700, Bethesda, MD 20892-3700. Tel.: 301-814-8119; E-mail: Antonina@mail.nih.gov.

[2] The abbreviations used are: TAT, tubulin acetyltransferase; GNAT, GCN5-related *N*-acetyltransferases; Ac-CoA, acetyl-CoA; AU, asymmetric unit; r.m.s.d., root mean square deviations; AUC, analytical ultracentrifugation; Se-Met, selenomethionine.

Although the majority of tubulin posttranslational modifications concentrate on the tubulin C-terminal tails that decorate the outside of the microtubule, TAT is unusual as it acetylates Lys-40 of α-tubulin (15), a residue located in a flexible loop in the microtubule lumen (16). The location of the acetylated residue makes it puzzling to understand how acetylation can affect cellular effectors. One hypothesis is that this modification leads to subtle changes in the microtubule lattice that can affect binding of effectors and polymer dynamics. Consistent with this, ultrastructural analyses of microtubules in touch receptor neurons of mec-17 mutants show a variability in protofilament number when compared with wild-type and large lattice defects that cause microtubules to splay apart and compress radially (17, 18).

To provide a structural scaffold within which to better understand the mechanism of TAT, we determined the x-ray structure of an active core of TAT in complex with Ac-CoA. Structure-based mutagenesis reveals molecular determinants of tubulin acetylation. We also report the x-ray structure of an active site mutant that, unlike the wild-type protein, is a stable, inactive dimer in solution and crystallizes as a domain-swapped dimer, revealing unexpected plasticity of the N-terminal domain of TAT. We thus identify an intramolecular interface in TAT that is metastable and when destabilized leads to dimer and higher-order oligomer formation. Intriguingly, this metastable region is important for TAT activity and contains a conserved motif predicted to be important for substrate engagement in GNAT superfamily members. Our work shows that TAT contains a conserved, stable catalytic core and a structurally plastic N terminus important for function. Tubulin hyperacetylation is associated with neuronal injury (1, 19), making TAT an attractive target for small molecule inhibitors.

EXPERIMENTAL PROCEDURES

Protein Expression and Purification—Danio rerio TAT, residues 1–186, was expressed in *Escherichia coli* Rosetta2 (DE3) pLysS as a GST fusion. Protein expression was induced with 0.5 mM isopropyl-1-thio-β-D-galactopyranoside for 16 h at 16 °C. Cells were microfluidized, and cellular debris was removed by centrifugation at 100,000 × *g* for 50 min. The protein was bound to GST resin (GE Healthcare) and released by tobacco etch virus protease cleavage. TAT was further purified by anion exchange (MonoQ, GE Healthcare) and then concentrated and loaded on a HiLoad 16/60 S75 size exclusion column (GE Healthcare) pre-equilibrated in 20 mM Tris-HCl, pH 7.5, 200 mM NaCl, 5 mM $MgCl_2$, and 1 mM tris(2-carboxyethyl)phosphine. The Se-Met protein was expressed in a Met auxotroph strain and purified as above. *D. rerio* D117A TAT mutant, residues 1–196, was purified as above. All point mutants were made in the background of the 1–196 TAT construct.

Crystallization of D. rerio TAT—TAT and TAT D117A (in size-exclusion chromatography buffer) were mixed with 2-fold molar excess of Ac-CoA and concentrated to 10 g/liter by ultrafiltration. Crystals were obtained by vapor diffusion at 20 °C after mixing equal volumes of protein and reservoir solution (0.1 M MES, pH 6.5, 0.5–0.7 M NaH_2PO_4 and KH_2PO_4). For data collection, crystals were briefly transferred to the reservoir solution supplemented with 35% xylitol (w/v) and plunged into liquid nitrogen.

Structure Determination—Crystals have the symmetry of space group $P4_32_12$ and two TAT copies per asymmetric unit (AU) ($a = 81.5$ Å, $c = 117.7$ Å). Se-Met multiwavelength anomalous dispersion data were collected at the Advanced Light Source (ALS), Lawrence Berkeley National Laboratory, Beamline 5.0.2. (see Table 1). Five of the six possible selenium sites were found using SOLVE (20), and phases were calculated using CNS (21). The experimental electron density maps at this stage were not interpretable (mean overall figure of merit 0.306), but solvent flipping and histogram matching yielded maps in which ~60% of the protein could be built. Refinement of the partial model using PHENIX (22) and calculation of electron density maps with combined phases and later $(2|F_{obs}| - |F_{calc}|)\alpha_{model}$ difference Fourier syntheses allowed completion of protein structure building. Six regions of the polypeptide chains (copy A, residues 20–38, 49–68, and 80–82; copy B, residues 22–38, 50–68, and 78–84) are not well resolved in the electron density map and presumed disordered.

Crystals of TAT D117A have the symmetry of space group $P4_32_12$ and two TAT copies per AU ($a = 58.1$ Å, $c = 255.0$ Å). The structure was solved by molecular replacement using PHASER (23). Iterative model building and refinement were carried out in COOT (24) and PHENIX (22) (see Table 1). Three regions of the polypeptide chain (copy A, residues 48–67; copy B, residues 22–32 and 49–65) were not visible in the electron density maps and presumed disordered.

Acetyltransferase Activity Assays—Acetylation of porcine brain tubulin (Cytoskeleton) was assayed through the incorporation of the radiolabeled acetyl group from [^{3}H]Ac-CoA into tubulin as described (3). Reactions were assembled on ice in 80 mM PIPES-KOH, pH 6.9, 50 mM NaCl, 1 mM EGTA, 1 mM $MgCl_2$, 1 mM DTT, 20 μM [^{3}H]Ac-CoA (2.1 Ci/mmol), and 180 μM Ac-CoA, containing either 20 μM colchicine for tubulin or 1.6 M glycerol and 1 mM GTP for microtubule reactions. Reactions were initiated at room temperature by adding 1 μM TAT.

Analytical Ultracentrifugation—Sedimentation velocity analytical ultracentrifugation (AUC) experiments were performed at 20 °C in an XL-I ultracentrifuge (Beckman) using absorption optics. Peak fractions of TAT from size-exclusion chromatography were used. Data were collected and analyzed as described (25). For all cases, good fits were obtained with root mean square deviations (r.m.s.d.) between 0.003 and 0.004. The higher molecular weight species are due to an impurity and do not vary as a percentage of total absorbance as a function of TAT concentration.

RESULTS

Structural Overview of the Active TAT Core—We isolated a stable, monodisperse fragment of *D. rerio* TAT (residues 1–186) that acetylates porcine brain tubulin *in vitro* at a rate of $0.4\ h^{-1}$, comparable with that of the full-length human enzyme, and retains the enhancement in activity observed with microtubules for the full-length TAT (Fig. 1*A*) (3). This construct produced diffraction-quality co-crystals, with two crystallographically independent copies of the 1:1 protein:ligand com-

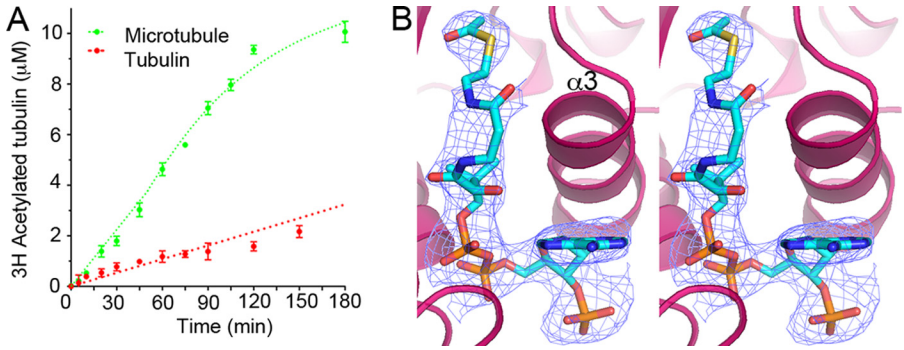

FIGURE 1. **TAT truncation is active**. *A*, acetylation time course of monomeric tubulin (*red*) and microtubules (*green*) by TAT, residues 1–186. *B*, stereo view showing bound Ac-CoA as stick model and $2|F_o| - |F_c|$ composite anneal-omit electron density contoured at 1.0σ (*blue*). *Error bars* indicate S.E. ($n \geq 3$).

plex in the AU (see "Experimental Procedures" and Table 1), with well defined electron density for the Ac-CoA (Fig. 1*B*).

The structure of Ac-CoA-bound TAT is shown in Fig. 2*A*. The two TAT·Ac-CoA complexes in the AU are very similar, with r.m.s.d. between their main-chain atoms of 0.4 Å, comparable with our crystallographic coordinate precision. Packing between the protomers is mediated by hydrogen bonds and van der Waals interactions, burying 1402 Å^2 of solvent-accessible surface area per protomer (26). Despite the considerable intermolecular buried area in this crystalline form, TAT is a monomer in solution at lower concentrations as demonstrated by AUC (Fig. 2*B*).

TAT is elongated, with dimensions of 30 × 62 × 30 Å^3 (width × height × depth in Fig. 2*A*), and composed of a curved, five-stranded β-sheet of mixed polarity surrounded by three α-helices and two 3_{10} helices. The structure resembles a cupped hand with the β-sheet forming the palm and the N-terminal β1-β2 hairpin forming the thumb. The Ac-CoA is cradled in a shallow groove between β7 on one side and α3 and the α3-β8 loop on the other. The β1 and β2 strands complete an extended β-sheet belonging to the neighboring protomer, with β1 participating in the dimerization interface of the TAT noncrystallographic dimer. At the tip of the cupped hand lies a conserved β-hairpin formed of strands β5-β6 and supported by a network of invariant phenylalanine residues; the invariant Phe-184 makes π-stacking interactions with the invariant Phe-183 and van der Waals contacts with conserved Leu-171 and Leu-100 (Fig. 2*C*). Interestingly, the residues in the C-terminal 3_{10}-2 helix and the preceding β9 form one of the most conserved sequence stretches outside the four GNAT superfamily motifs (supplemental Fig. 1). This structural motif is unique to TAT and not found in other GNAT superfamily members of known structure.

At the N terminus, α1 packs against the core β-sheet on one side and makes a network of hydrophobic interactions with residues in β2 on the other; invariant Phe-11 packs against conserved Phe-3 and Leu-45, and conserved Ile-42 makes van der Waals interactions with Phe-3 (Fig. 2*D*). Consistent with the importance of these interactions, a 10-residue N-terminal deletion in TAT decreases activity dramatically, and mutation L45A reduces activity by 70% (3) (data not shown). Two stretches of residues on either side of β2 (residues 22–38 and 50–68) lack electron density in this wild-type crystal structure and are presumed disordered. In structures of other GNAT

TABLE 1
Crystallographic data and refinement statistics

$R_{sym} = \Sigma I - \langle I \rangle / \Sigma I$, where I = observed intensity, $\langle I \rangle$ = average intensity obtained from multiple observations of symmetry related reflections. r.m.s. bond lengths and r.m.s. bond angles are the respective root mean square deviations from ideal values. Free R factor was calculated with 5% of data omitted from the structure refinement.

	TAT (Se-Met)[a]		
	Inflection	Remote	D117A TAT[a]
Data collection			
Wavelength (Å)	0.9806	0.9637	1.0
Resolution (Å)	2.70 (2.75–2.70)	2.70 (2.75–2.70)	2.45 (2.49–2.45)
R_{sym}	9.8 (78.0)	9.4 (56.4)	10.9 (50.4)
$\langle I \rangle / \langle \sigma(I) \rangle$	22.5 (1.8)	24.9 (2.6)	33.6 (3.6)
Completeness (%)	100.0 (100.0)	100.0 (100.0)	99.9 (99.9)
Redundancy	6.9 (6.5)	7.0 (7.1)	11.4 (10.8)
Wilson B-factor	59.6	54.3	45.7
Refinement			
Resolution (Å)		47.7–2.70	29.06–2.45
No. of reflections		11419	15066
R_{work}/R_{free} (%)		22.1/23.8	19.6/24.8
No. of atoms			
Protein/ligand		2315/102	2543/102
Ion/water		10/13	6/41
Mean B-factors (Å^2)			
Protein/ligand		45.1/46.3	49.0/48.3
Ion/water		66.4/38.4	59.2/43.3
r.m.s.d. (bond (Å)/ angles (°))		0.005/0.853	0.015/1.52
Ramachandran plot			
Most favored		96.1%	97.3%
Disallowed		0.6%	0.0%

[a] Values in parentheses are for highest resolution shell.

superfamily members, the N-terminal region comprising Motif C clasps the Ac-CoA binding site, making stabilizing interactions with the pantothenic acid of the Ac-CoA and the peptide substrate (27).

Mapping sequence conservation of TAT family members onto the crystal structure reveals that core secondary structural elements are conserved, with residues supporting the active site being most conserved (Fig. 2*A* and supplemental Fig. 1). Despite having only 11% overall sequence identity with GCN5, the TAT core comprising the three-stranded β-sheet (β3, β4, and β7) and helices α2 and α3 shows strong structural equivalencies with the corresponding region in GCN5 (28) and other GNAT superfamily members (r.m.s.d. with GCN5 = 3.2 Å over residues 70–180). However, the structural similarity does not extend to the N terminus or the β5-β6 hairpin and C-terminal phenylalanine-rich motif unique to TAT.

Active Site Architecture and Molecular Determinants of Tubulin Acetylation—Ac-CoA binds in a shallow conserved groove, flanked by residues in Motifs A (β7, α2, and the con-

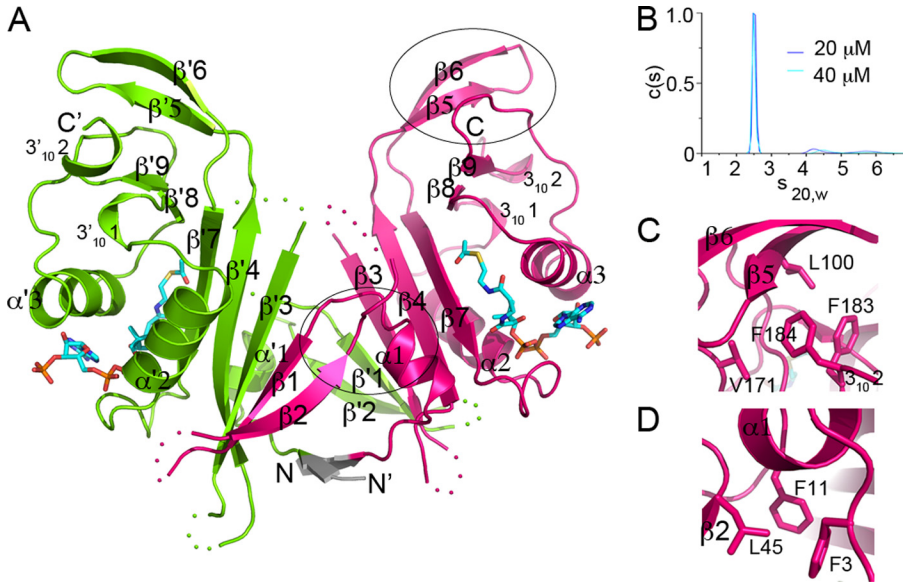

FIGURE 2. **Crystal structure of TAT.** *A*, ribbon representation of the TAT crystal structure bound to Ac-CoA; the latter is shown as a stick model. *Colored dots* represent regions of the polypeptide chain that are disordered in the crystal. *B*, TAT is a monomer in solution. Sedimentation coefficient distributions c(*s*) at 20 (*blue*) and 40 μM (*cyan*) are shown. *C*, conserved C-terminal phenylalanine-rich motif (*circled* in *A*, *upper right*). *D*, conserved hydrophobic network at the N terminus (*circled* in *A*, *center*).

necting loop) and B (β8, α3, and the connecting loop) (Fig. 3*A*). Unlike in other GNAT superfamily member structures (27), the adenine moiety of the CoA is well ordered in our TAT structure. The angle of the glycosidic bond places the nucleobase in an orientation intermediate between canonical *anti* and *syn* conformations. The purine base is sandwiched between the guanidinium of invariant Arg-126 and aliphatic side chain of invariant Lys-156. The 3′-phosphate of the adenosyl moiety is held by salt bridges with the side chains of Arg-126 and Lys-163 (Fig. 3*A*). The pyrophosphate of Ac-CoA is coordinated predominantly by hydrogen bonds with main-chain atoms belonging to the highly conserved Arg/Gln-*X*-*X*-Gly-*X*-Gly segment of Motif A (supplemental Fig. 1) in the loop preceding α2. The pantoic acid moiety is cradled in a shallow pocket lined by the side chains of invariant phenylalanines: Phe-118, Phe-157, and Phe-160. Invariant Ser-154 of Motif B hydrogen-bonds to the carbonyl of the amide linking the β-alanine and β-mercaptoethylamine moieties of Ac-CoA. Finally, the carbonyl of the acetyl group itself hydrogen-bonds to the main-chain amide of Phe-157 (Fig. 3*A*). Consistent with the Ac-CoA coordination observed in our structure, mutation of Arg-126 or Ser-154 reduced activity to 19 and 8% of wild-type, respectively. Mutation of variable Ser-131 that hydrogen-bonds with the pyrophosphate of Ac-CoA had no effect on activity (Fig. 3*B*).

Examination of the surface conservation around the Ac-CoA binding site reveals two invariant aspartates (Asp-117 and Asp-151) in close proximity to the acetyl moiety where they could participate in substrate coordination. Consistent with this, their mutation reduces activity drastically (D117A has 3% of wild-type activity, whereas D151A has 1%). Further analysis of the structure suggests additional residues that might be important for substrate recognition: Arg-152 that forms a salt bridge with Asp-151 as well as His-70 and Lys-96 that lie further away from the acetyl group at the edge of a shallow conserved canyon that could accommodate the tubulin loop.

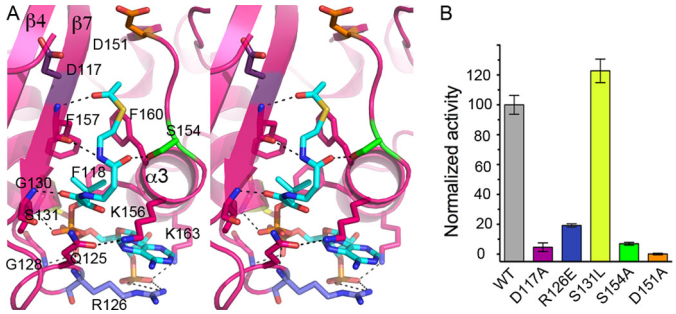

FIGURE 3. **Active site architecture.** *A*, stereo view of the active site. *B*, normalized tubulin acetylation activity of structure-guided TAT mutants color-coded to match residue colors in *A*. *Error bars* indicate S.E. ($n \geq 3$).

Crystal Structure of an Inactive Mutant Reveals Extraordinary Plasticity of the TAT N Terminus—While investigating the contribution of residues proximal to the Ac-CoA binding site, we discovered that the inactive D117A mutant (Fig. 3*B*) is a constitutive dimer in solution (Fig. 4). To understand the basis for this oligomerization, we determined its crystal structure at 2.45 Å resolution (see "Experimental Procedures" and Table 1). Like that of the wild type, the AU of the D117A crystal contains two protomers (Fig. 4*A*) that are structurally very similar with r.m.s.d. between main-chain atoms of 0.4 Å. The TAT D117A core is structurally similar to that of the wild type (Figs. 2*A* and 4*A*) and superimposes with a main-chain r.m.s.d. of 0.4 Å over residues 70–184. Ac-CoA binds as in the wild-type structure.

Strikingly, the D117A mutant is domain-swapped, with α1 and β1 contributed by the other protomer of the dimer. In the D117A structure, residues 24–38, which were disordered in the wild-type structure, are clearly seen to wrap around the base of the dimer in an extended structure comprising helix α1a and strand β1a as well as 9 residues with irregular structure (supplemental Fig. 1). Strand β2 is 3 residues shorter than in the wild-type structure and forms only a 3-residue-long backbone hydrogen-bonded network with β′1 (Fig. 4*A*). As a result,

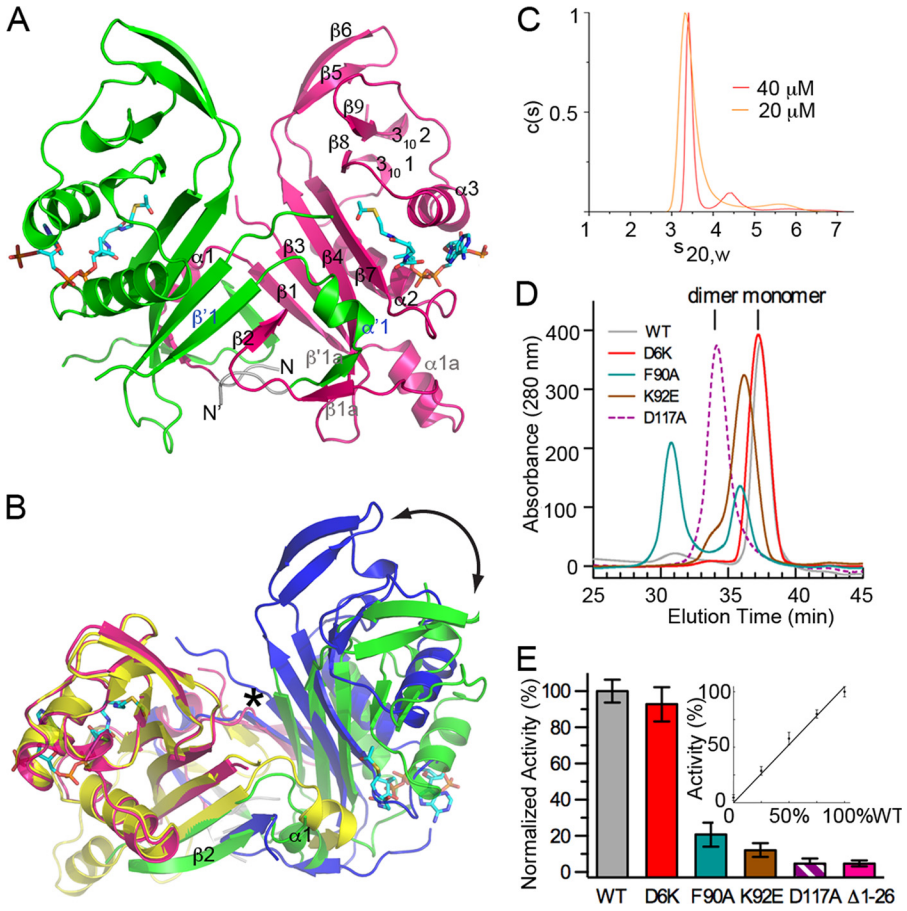

FIGURE 4. **The TAT N terminus is essential and structurally plastic.** *A*, ribbon representation of the D117A TAT crystal structure bound to Ac-CoA colored as in Fig. 2*A*. *B*, superposition of wild-type and D117A TAT structures. *Green* (protomer A) and *magenta* (protomer B), wild-type TAT crystallographic dimer; *yellow* (protomer A) and *blue* (protomer B), D117 A TAT dimer. Swapped elements are labeled in *blue*. *, pivot point. *C*, D117A TAT is a dimer in solution. Sedimentation coefficient distributions c(*s*) at 20 (*orange*) and 40 μM (*red*) are shown. *D*, mutants at the α1/central β-sheet interface result in higher-order oligomers as assayed by size-exclusion chromatography. Void volume, 17 min. *E*, normalized tubulin acetylation activity of TAT mutants color-coded to match the traces in *D*. *Error bars* indicate S.E. ($n \geq 3$). *Inset*: normalized tubulin acetylation activity of 0/100, 25/75, 50/50, and 100/0% wild-type/D117A TAT mixtures.

although conserved Ile-42 forms part of the β1-β2 hairpin in the wild-type structure, it is now at the C-terminal end of the irregular polypeptide segment preceding β2 that wraps around the base of the dimer. The network of hydrophobic interactions between residues in α1 and β2 (β'2 in D117A) is similar, with Leu-45 making van der Waals interactions with Phe-3 and Phe-11 (Fig. 2*D*); however, now the latter residues belong to the other protomer. These residues are now therefore part of the dimerization interface. Interestingly, β2 contains the longest stretch of conserved residues outside the GNAT superfamily Motifs A and B directly involved in Ac-CoA binding and the β5-β6 TAT family-specific β-hairpin and is predicted to be part of Motif C involved in substrate recognition in GNAT family members (13). In D117A, the total buried surface area per protomer is 2610 Å^2. The increase in buried area by ~1200 Å^2 explains the propensity of this mutant to dimerize in solution (Fig. 4, *C* and *D*). Consistent with the stability of the dimer, we do not observe any monomeric species even at lower concentrations (5 μM) by AUC (data not shown), and when the inactive mutant dimer is mixed with the wild-type construct, there is no inhibition of the activity of the wild-type construct (Fig. 4*E*).

Superposition of the core (residues 70–185) of one protomer from the wild-type and the D117A TAT structures reveals that the second protomer rotates by ~15° with respect to the wild-type protomer (Fig. 4*B*). The hinge lies in proximity to Pro-12, at the interface between the core β-sheet and the loop between α1 and β1. Pro-12 appears to make stabilizing van der Waals contacts with Asp-117 in the wild-type structure. The functional importance of the N-terminal region comprising α1 and β1 is underscored by the fact that an N-terminal truncation is severely impaired in acetylating tubulin (Fig. 4*E*). Consistent with this destabilization of intramolecular contacts, several other point mutations at the interface between the core β-sheet and the α1-β1 loop (F90A, where Phe-90 makes stabilizing van der Waals contacts with Phe-11, Leu-7, and Pro-12, and K92E, where Lys-96 hydrogen-bonds with the backbone carbonyl of Pro-12) result in various degrees of higher-order oligomerization, whereas a mutation in α1 that is not part of this interface (D6A) does not (Fig. 4*D*). The F90A and K92E mutants also have drastically reduced activities (Fig. 4*E*).

DISCUSSION

The three-dimensional structure of this unusual acetyltransferase reveals the overall architecture of TAT and identifies active-site residues important for tubulin acetylation. Our structure of an active site mutant that, unlike the wild-type

protein, is a stable, inactive dimer in solution reveals a domain swap and underscores the structural plasticity of the functionally essential TAT N-terminal domain. We identify an intramolecular interface in TAT that is metastable and when destabilized leads to dimer and higher-order oligomer formation and impaired activity.

The structurally plastic region contains Motif C predicted to be important for substrate engagement in GNAT superfamily members. Surprisingly, the structurally equivalent region in GNAT members is α-helical (27, 29), unlike in our structure, where it is a β-strand (β2). In the monomeric state in solution and in the absence of substrate, this region of TAT is most likely structurally labile and able to adopt variable conformations. TAT is quite unusual as an acetyltransferase as it has an extremely low basal activity with tubulin (0.4 h^{-1}), and even after ~8-fold enhancement by the microtubule lattice, its activity is 50 times less than that of GCN5, the prototypical GNAT superfamily member (30). Its low basal activity with tubulin is similar to that of the histone acetyltransferase Rtt109 (0.1 h^{-1} (30)). Rtt109 maximal activity requires the association of two histone chaperones, Vps75 or Asf1, that stabilize the catalytically active conformation of the enzyme (31). In the case of TAT, the microtubule lattice could be functioning as the chaperone stabilizing its catalytically active conformation. Different organisms and cell types have microtubules with variable protofilament numbers, and TAT has evolved to function with these varying polymer architectures (17). This functional plasticity could be related to the structural plasticity that we have uncovered.

Our work represents a starting point for further crystallographic, biochemical, and genetic studies of members of the TAT family that should aid systematic analyses of the mechanism by which TAT accesses the microtubule lumen and has its activity enhanced by the microtubule. Recent studies show that microtubule deacetylation at the site of axonal injury is essential for the regeneration potential of the axon (32); thus TAT inhibitors are attractive targets for potential applications in neuronal injury repair. Our crystal structure should aid in such future endeavors.

Acknowledgments—We thank the staff at ALS sector 5 for data collection support and N. Ziolkowska for help with molecular biology and protein expression. A. R. M. thanks A. Deaconescu, A. Ferré-D'Amaré, and S. Gottesman for support and critical reading of the manuscript.

REFERENCES

1. Garnham, C. P., and Roll-Mecak, A. (2012) The chemical complexity of cellular microtubules: tubulin post-translational modification enzymes and their roles in tuning microtubule functions. *Cytoskeleton* **69,** 442–463
2. Wloga, D., and Gaertig, J. (2010) Post-translational modifications of microtubules. *J. Cell Sci.* **123,** 3447–3455
3. Shida, T., Cueva, J. G., Xu, Z., Goodman, M. B., and Nachury, M. V. (2010) The major α-tubulin K40 acetyltransferase αTAT1 promotes rapid ciliogenesis and efficient mechanosensation. *Proc. Natl. Acad. Sci. U.S.A.* **107,** 21517–21522
4. Akella, J. S., Wloga, D., Kim, J., Starostina, N. G., Lyons-Abbott, S., Morrissette, N. S., Dougan, S. T., Kipreos, E. T., and Gaertig, J. (2010) MEC-17 is an α-tubulin acetyltransferase. *Nature* **467,** 218–222
5. L'Hernault, S. W., and Rosenbaum, J. L. (1983) *Chlamydomonas* α-tubulin is posttranslationally modified in the flagella during flagellar assembly. *J. Cell Biol.* **97,** 258–263
6. Gaertig, J., Cruz, M. A., Bowen, J., Gu, L., Pennock, D. G., and Gorovsky, M. A. (1995) Acetylation of lysine 40 in α-tubulin is not essential in *Tetrahymena thermophila*. *J. Cell Biol.* **129,** 1301–1310
7. Hammond, J. W., Huang, C. F., Kaech, S., Jacobson, C., Banker, G., and Verhey, K. J. (2010) Posttranslational modifications of tubulin and the polarized transport of kinesin-1 in neurons. *Mol. Biol. Cell* **21,** 572–583
8. Reed, N. A., Cai, D., Blasius, T. L., Jih, G. T., Meyhofer, E., Gaertig, J., and Verhey, K. J. (2006) Microtubule acetylation promotes kinesin-1 binding and transport. *Curr. Biol.* **16,** 2166–2172
9. Santander, V. S., Bisig, C. G., Purro, S. A., Casale, C. H., Arce, C. A., and Barra, H. S. (2006) Tubulin must be acetylated in order to form a complex with membrane Na^+,K^+-ATPase and to inhibit its enzyme activity. *Mol. Cell. Biochem.* **291,** 167–174
10. Friedman, J. R., Webster, B. M., Mastronarde, D. N., Verhey, K. J., and Voeltz, G. K. (2010) ER sliding dynamics and ER-mitochondrial contacts occur on acetylated microtubules. *J. Cell Biol.* **190,** 363–375
11. Piperno, G., and Fuller, M. T. (1985) Monoclonal antibodies specific for an acetylated form of α-tubulin recognize the antigen in cilia and flagella from a variety of organisms. *J. Cell Biol.* **101,** 2085–2094
12. L'Hernault, S. W., and Rosenbaum, J. L. (1985) *Chlamydomonas* α-tubulin is posttranslationally modified by acetylation on the ϵ-amino group of a lysine. *Biochemistry* **24,** 473–478
13. Steczkiewicz, K., Kinch, L., Grishin, N. V., Rychlewski, L., and Ginalski, K. (2006) Eukaryotic domain of unknown function DUF738 belongs to Gcn5-related *N*-acetyltransferase superfamily. *Cell Cycle* **5,** 2927–2930
14. Neuwald, A. F., and Landsman, D. (1997) GCN5-related histone *N*-acetyltransferases belong to a diverse superfamily that includes the yeast SPT10 protein. *Trends Biochem. Sci.* **22,** 154–155
15. LeDizet, M., and Piperno, G. (1987) Identification of an acetylation site of *Chlamydomonas* α-tubulin. *Proc. Natl. Acad. Sci. U.S.A.* **84,** 5720–5724
16. Nogales, E., Wolf, S. G., and Downing, K. H. (1998) Structure of the αβ tubulin dimer by electron crystallography. *Nature* **391,** 199–203
17. Topalidou, I., Keller, C., Kalebic, N., Nguyen, K. C., Somhegyi, H., Politi, K. A., Heppenstall, P., Hall, D. H., and Chalfie, M. (2012) Genetically separable functions of the MEC-17 tubulin acetyltransferase affect microtubule organization. *Curr. Biol.* **22,** 1057–1065
18. Cueva, J. G., Hsin, J., Huang, K. C., and Goodman, M. B. (2012) Posttranslational acetylation of α-tubulin constrains protofilament number in native microtubules. *Curr. Biol.* **22,** 1066–1074
19. Chen, L., and Rolls, M. M. (2012) Microtubule deacetylation sets the stage for successful axon regeneration. *EMBO J.* **31,** 3033–3035
20. Terwilliger, T. C., and Berendzen, J. (1999) Automated MAD and MIR structure solution. *Acta Crystallogr. D Biol. Crystallogr.* **55,** 849–861
21. Brünger, A. T., Adams, P. D., Clore, G. M., DeLano, W. L., Gros, P., Grosse-Kunstleve, R. W., Jiang, J. S., Kuszewski, J., Nilges, M., Pannu, N. S., Read, R. J., Rice, L. M., Simonson, T., and Warren, G. L. (1998) Crystallography & NMR system: A new software suite for macromolecular structure determination. *Acta Crystallogr. D Biol. Crystallogr.* **54,** 905–921
22. Adams, P. D., Afonine, P. V., Bunkóczi, G., Chen, V. B., Davis, I. W., Echols, N., Headd, J. J., Hung, L. W., Kapral, G. J., Grosse-Kunstleve, R. W., McCoy, A. J., Moriarty, N. W., Oeffner, R., Read, R. J., Richardson, D. C., Richardson, J. S., Terwilliger, T. C., and Zwart, P. H. (2010) PHENIX: a comprehensive Python-based system for macromolecular structure solution. *Acta Crystallogr. D Biol. Crystallogr.* **66,** 213–221
23. McCoy, A. J., Grosse-Kunstleve, R. W., Adams, P. D., Winn, M. D., Storoni, L. C., and Read, R. J. (2007) Phaser crystallographic software. *J. Appl. Crystallogr.* **40,** 658–674
24. Emsley, P., and Cowtan, K. (2004) Coot: model-building tools for molecular graphics. *Acta Crystallogr. D Biol. Crystallogr.* **60,** 2126–2132
25. Szyk, A., Deaconescu, A. M., Piszczek, G., and Roll-Mecak, A. (2011) Tubulin tyrosine ligase structure reveals adaptation of an ancient fold to bind and modify tubulin. *Nat. Struct. Mol. Biol.* **18,** 1250–1258
26. Lee, B., and Richards, F. M. (1971) The interpretation of protein structures: estimation of static accessibility. *J. Mol. Biol.* **55,** 379–400
27. Dyda, F., Klein, D. C., and Hickman, A. B. (2000) GCN5-related *N*-acetyl-

transferases: a structural overview. *Annu. Rev. Biophys. Biomol. Struct.* **29,** 81–103
28. Rojas, J. R., Trievel, R. C., Zhou, J., Mo, Y., Li, X., Berger, S. L., Allis, C. D., and Marmorstein, R. (1999) Structure of *Tetrahymena* GCN5 bound to coenzyme A and a histone H3 peptide. *Nature* **401,** 93–98
29. Trievel, R. C., Rojas, J. R., Sterner, D. E., Venkataramani, R. N., Wang, L., Zhou, J., Allis, C. D., Berger, S. L., and Marmorstein, R. (1999) Crystal structure and mechanism of histone acetylation of the yeast GCN5 transcriptional coactivator. *Proc. Natl. Acad. Sci. U.S.A.* **96,** 8931–8936
30. Berndsen, C. E., and Denu, J. M. (2008) Catalysis and substrate selection by histone/protein lysine acetyltransferases. *Curr. Opin. Struct. Biol.* **18,** 682–689
31. Kolonko, E. M., Albaugh, B. N., Lindner, S. E., Chen, Y., Satyshur, K. A., Arnold, K. M., Kaufman, P. D., Keck, J. L., and Denu, J. M. (2010) Catalytic activation of histone acetyltransferase Rtt109 by a histone chaperone. *Proc. Natl. Acad. Sci. U.S.A.* **107,** 20275–20280
32. Cho, Y., and Cavalli, V. (2012) HDAC5 is a novel injury-regulated tubulin deacetylase controlling axon regeneration. *EMBO J.* **31,** 3063–3078